AIAA JOURNAL
Vol. 46, No. 6, June 2008

Feasibility Study for Steering a Supersonic Projectile by a Plasma Actuator

Patrick Gnemmi,* Romain Charon,† Jean-Pierre Dupéroux,† and Alfred George‡
French–German Research Institute of Saint-Louis, 68301 Saint-Louis Cedex, France

DOI: 10.2514/1.24696

Experimental and theoretical investigations on the possibilities of steering a supersonic projectile by using a plasma actuator started in 2001, but they have not been published up to now, for confidentiality reasons. The experimental study shows the possibility of activating plasma discharges at the tip of a supersonic projectile flying in conditions encountered at a low altitude. Plasma discharges were produced by the use of high-voltage generators that were able to supply electric discharges between two electrodes flush with the conical surface of the projectile nose. Visualizations show that the generation of a plasma discharge produces a perturbation between the projectile surface and the shock wave attached to the conical projectile tip. The perturbation is strong enough to distort the shock wave. A numerical simulation was performed for an ideal gas, in which the plasma discharge was modeled as a transverse hot jet. The comparison between the flow visualizations and the numerical results shows the similarity between the visualized and the computed flow structures. The results show that the asymmetry of the flowfield around the projectile produces a lateral force and a pitching moment that favorably combine to steer the projectile.

Nomenclature

B	=	magnetic field, T
D	=	projectile caliber, m
F	=	force, N
Fn	=	normal force, N
Fp	=	thrust force, N
Fx	=	drag force, N
I	=	current intensity, A
j	=	current density, A/m^2
M	=	Mach number
$My/0$	=	pitching moment at projectile tip, mN
P	=	static pressure, Pa
p	=	pressure, Pa
r	=	radius, m
S_p	=	plasma area, m^2
T	=	static temperature, K
t	=	time, s
U	=	electric voltage, V
v_{jet}	=	jet velocity, m/s
Xcp	=	abscissa of the center of pressure, m
μ_0	=	magnetic permeability ($4\pi \times 10^{-7}$ for the air), H/m
ρ	=	density, kg/m^3

I. Introduction

THE trajectory change of a flying vehicle is made possible by unbalancing the pressures acting on the body surface. This pressure asymmetry may be produced by surface deployment or by the use of one or more pyrotechnical mechanisms judiciously distributed on the vehicle. The major drawback when using the surface-spreading technique is that it involves large forces to deploy the surfaces to overcome the very large pressures encountered at high-speed velocities. Thus, the use of pyrotechnical mechanisms is more appropriate for high-speed vehicles, but the fact that the pyrotechnical mechanism works only once and produces everything or nothing is a main drawback when an angle of attack must be given to a high-speed vehicle.

Joint studies performed at the French–German Research Institute of Saint-Louis (ISL) and at the Defence Research Establishment of Valcartier, Canada (DREV), on the use of projectile fins have been going on for a few years. The principle of using fins is applied to subsonic projectiles [1] and high transonic projectiles ($M \leq 1.5$) [2–4]. The application of that concept to supersonic projectiles ($M \leq 3.0$) has led to the development of the grid-fin concept, also studied at ISL and DREV [5]. A recent study of the use of grid fins on a hypersonic missile has started at ISL in cooperation with EADS-LFK GmbH (Unterschleissheim, Germany) [6]. Other studies, in which ISL, Rheinmetall Landsysteme GmbH (Unterlüss, Germany), and DLR (German Aerospace Center, Köln-Porz, Germany) are involved, deal with the use of lateral jets to laterally move supersonic or hypersonic projectiles and missiles [7–11]. All of these studies treat the theoretical and experimental aspects of the problem.

A study concerning the means of antiaerial fight started at ISL during the year 2001. It concerns the increase of the projectile precision faced with increasingly agile aerial vehicles. The underlying idea consists of giving the antiaerial projectile a maneuvering capacity, allowing it to compensate for the trajectory prediction error. ISL suggests an innovative concept to deviate a projectile from an initial trajectory by giving a controlled angle of attack to the projectile. The studies relating to the application of this concept to the antiaerial projectile of mean caliber (≤ 40 mm) are grouped together in an ISL project called the Guided Supersonic Projectile (GSP) [12]. In the context of this project, the examination of solutions for steering a supersonic projectile flying at $M = 3$ reveals the need for at least one fast trajectory correction of large amplitude [12]. That correction necessitates several impulses to deviate and then stabilize the projectile on the new trajectory. In principle, for a conventional projectile, the more the flow perturbation due to an impulse is generated near its tip, the smaller the amplitude must be to obtain a given angle of attack; this is all the more so as the projectile flies near its stability limit.

The idea of generating electrical discharges to create a plasma at the projectile tip was born from the analysis of the different solutions for steering the GSP; a patent describing the concept and the system was filed in France in February 2002 and was issued in January 2005 [13]. The patent was published in many other countries and it was issued in the United States in February 2006 [14].

Received 19 April 2006; revision received 12 October 2007; accepted for publication 21 January 2008.

*Senior Scientist, Aerodynamics and External Ballistics Department; patrick.gnemmi@isl.eu. Senior Member AIAA.
†Engineer, Electromagnetic Waves Department.
‡Engineer, Aerothermodynamics and Shock Tube Department.

In an international context, the research work on the use of a plasma for flow control concerning aerial vehicles continues to increase. The most recent works on that subject are mentioned hereafter. The technology to reduce the drag of supersonic aerial vehicles [15,16] has been studied for many years. An actuator allowing the control of a supersonic flow at a low pressure is under investigation [17]. The influence of a plasma on a shock wave in a supersonic flow is also examined [18–20]. The effect of a plasma-assisted ignition on a high-speed flow is also being studied [21]. The airflow control in boundary layers is under study [22,23], and a system designed to delay the dynamic stall of a wing [24] is a concrete application of the technology at a subsonic speed. Other studies that have nothing to do with the work presented in this paper concern the furtive aspects of the flying vehicles faced with radar. In fact, a plasma surrounding a flying vehicle can absorb the electromagnetic waves under particular conditions, reducing the radar echo of that vehicle [25].

The work described in this paper concerning the possibility of giving an angle of attack to a projectile by plasma discharges is quite original (supersonic flow and low atmosphere, which means a high-pressure medium), because no application of this type presently exists.

II. Principle of the Concept

In the case of a high-speed vehicle, a shock wave occurs at its nosetip or ahead of it, depending on the nose geometry. When the vehicle flies without any angle of attack, the pressures distributed on its surface balance one another and the shock wave has symmetries that depend on the vehicle geometry. For example, for a supersonic projectile forebody with a conical nose, the shock wave is attached to the cone tip and is itself of conical shape. The proposed concept consists of producing the asymmetry of the flow variables around the projectile nose by generating one or several plasma discharges at the nosetip to give an angle of attack to the projectile.

Some theoretical investigations (see Sec. V) illustrate the feasibility of such a system. Figure 1 presents the qualitative result of a numerical computation of the projectile forebody, flying from right to left near the ground level at a Mach number of 3.2. A plasma discharge modeled as a transverse hot jet is applied near the nosetip during a certain length of time. The figure shows the forebody and the halves of two surfaces. The surfaces represent a constant pressure in the flowfield that is chosen to highlight the main structure of the latter. The attached shock wave is perfectly visible at the tip of the conical nose, as is the Prandtl–Meyer expansion wave at the junction of the conical nose with the cylindrical part of the forebody. On the side of the conical nose on which the plasma discharge is activated, the geometry of the shock wave is clearly distorted, due to the generation of the plasma discharge. On the contrary, on the opposite side, the geometry of the shock wave remains unperturbed.

The final objective consists of the production of one or several plasma discharges so that the asymmetry is large and long enough to cause the deviation of the projectile facing its initial trajectory. The absence of mobile parts and the repetitive action of discharges are the main advantages of this technique. In fact, the control of the vehicle can be realized by repetitive discharges activated on demand, depending on the required trajectory.

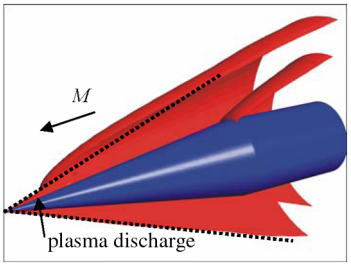

Fig. 1 Surfaces of constant pressure in the flowfield of a supersonic projectile forebody with a modeled plasma-discharge action.

III. Experimental Setup and Instrumentation

The experiments are carried out in the ISL shock-tube laboratory, which has two high-pressure shock tubes with a 100-mm inner diameter and a total length of about 30 m each [26–28]. The shock-tube facility works as a shock tunnel in which the shock-tube flow is expanded inside a circular parallel flow nozzle operating in the reflected mode. That facility is mainly used for experimentally investigating the flowfield around projectiles or missiles.

A. Shock-Tube Facility

The shock tunnel consists of a high-pressure driver tube, a driven tube, and a circular parallel flow nozzle attached to the end of the shock tube, as shown in Fig. 2. A steel diaphragm separates the hydrogen- or helium-filled driver tube from the air-filled driven tube. A Mylar diaphragm isolates the driven tube from the nozzle. The driver gas pressure reaches up to 60 MPa, and the initial driven gas pressure varies between 100 and 600 kPa. After diaphragm bursting, a shock wave is generated inside the driven tube and moves toward the end of the shock tube. At the nozzle throat, the incident shock wave is reflected, generating a quiescent high-pressure and high-temperature gas volume in front of the nozzle. This gas is expanded and accelerated inside the nozzle in such a way that the desired flight conditions are present at the nozzle exit during 3 to 4 ms. The atmospheric flight conditions can be duplicated in the ISL shock-tube facility, ranging from ground level up to more than 10 km of altitude. To reproduce the flight conditions in the test facility, the body is fixed inside a test chamber at the front of the nozzle and the airflow is accelerated to the desired pressure, temperature, and flight velocity.

B. Projectile Model

The projectile model has a conical nose with a 60-mm length and a cylindrical part with a 20-mm diameter. Two electrodes forming a plasma actuator are embedded in a vinyl polychloride part of the conical nose; they are located near the tip of the projectile model. One or two plasma discharges are generated between these two electrodes. The electrodes are identical: each electrode flush with the surface consists of a special conductor allowing the use of a high voltage (up to 18 kV). The distance between the electrodes is about 5 mm, allowing the production of a quasi-linear discharge. The electrodes could be arranged according to the longitudinal axis of the projectile model or perpendicularly to it. The choice of the electrode disposition is dictated by the results of previous numerical simulations: they show a better efficiency in terms of shock-wave deviation for the longitudinal axis alignment. Figure 3 shows a picture of the slightly eroded tip of the projectile model taken after a series of tests.

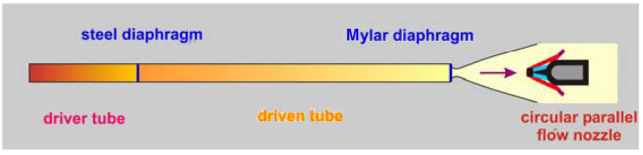

Fig. 2 Principle sketch of the shock-tunnel facility.

Fig. 3 Eroded tip of the projectile after tests.

C. High-Voltage Impulse Generator for Plasma Discharges

One or two plasma discharges are generated by the strain of one or two high-voltage impulses applied between the electrodes located near the projectile model's tip. A voltage measurement is carried out by means of a high-voltage probe with a 100-MHz bandwidth. The probe is connected to a Tektronix TDS 3054 oscilloscope, capable of recording 5-G samples per second.

1. Single Plasma Discharge

The high-voltage impulse generator used for the production of the plasma discharge was conceived and developed at ISL [29]. This type of apparatus is able to produce a voltage impulse by a Marx generator with a charge voltage of 10 kV per stage. The Marx generator is a voltage multiplier assembly of several stages for which the multiplication is obtained by the association of capacitors charged in parallel and then discharged in series by means of bursting. A two-stage generator is used for our application, to obtain a maximum impulse of 20 kV. The condensers have a capacity of 1.3 nF. Charged at 10 kV, they store an energy of 0.1 J, which is partially distributed during the impulse. The length of time necessary for the generation of the impulse, linked to the strain of bursting, is about 30 ns. The impulse duration is determined by the load of the circuit. The output of the generator is connected to a base fixed to a measurement chamber wall of the shock tube, close to the projectile model. The inner connection between that base and the projectile model is ensured by a high-voltage wire of about a 1-m length.

2. Two Plasma Discharges

The high-voltage impulse generator is not programmed to deliver several consecutive impulses. In fact, the loading of the capacitors is too long to allow an adequate impulse rate during the experiment lasting for about 3 ms. This problem is solved by assembling two identical high-voltage impulse generators, similar to the generator used for the single plasma discharge. The generators, coupled to a common output, are triggered with different delays to obtain two consecutive impulses separated by an adjustable delay Δt_p. A series of diodes are mounted on the output of the second generator so that the first generator does not drive the second one. The size of the diode assembly is such that it could withstand the high voltage and the discharge current.

D. Flowfield Visualization

The projectile model is fixed in the test chamber of the shock tube, and when the flow is established around the model, it is quasi steady for 3 to 4 ms. During that time, the plasma discharge is produced at the projectile nosetip, a spark is generated through a differential interferometer (DI) system, and the flowfield structure is visualized by a Pixelfly CCD camera. The camera is equipped with a 100-mm lens and its shutter is opened during 200 μs.

The DI is used as a flow visualization technique [30] based on the density-gradient field to gather information about the flow pattern around the projectile model. Two perpendicularly polarized widened light bundles, which are separated by a prism, pass through the flowfield in parallel. They are separated from each other by a certain distance (tenths of a millimeter). The light beams are brought together by a second prism, analyzed by a polarizer, and focused on the CCD camera by a lens system. The density changes produced in the flowfield generate different optical path lengths between the two split light bundles, giving an interference pattern on the CCD camera. The DI can be adjusted to obtain fringe patterns or an infinite fringe width, showing a homogeneous light-intensity distribution. In this case, the pictures look like schlieren pictures. In this way, the density-gradient field in the gas flow is visualized in terms of the light-intensity distribution shown on interferogram pictures.

E. Experiment Synchronization

One photodiode is fixed opposite the plasma discharge, and the signal is recorded to verify the presence of the plasma discharge. Classical measurements are carried out in the shock tube during each test to get the experimental conditions of the steady-state flow.

1. Single Plasma Discharge

A series of sparks is generated during each experiment, but only one is used to get the flowfield structure. During the experiment, the shock-tube laboratory is darkened, the CCD camera shutter is opened, the plasma discharge is generated, the selected spark is produced, and the CCD camera shutter is closed. A delay Δt corresponds to the time interval between the plasma discharge and the selected spark. The variation of that delay allows the flow evolution to be followed after the plasma-discharge production. Figure 4a shows the synchronization of an experiment in diagrammatic form.

2. Two Plasma Discharges

Two plasma discharges separated by a delay Δt_p are delivered before the spark (used for the DI) fixes the flow-structure image on the CCD camera. The delay Δt_c corresponds to the time interval between the first plasma discharge and the selected spark. Figure 4b shows the synchronization of one experiment in diagrammatic form.

IV. Dynamic Effects in Electric Arcs

Electric discharges in gases (in other words, gas discharges) are generators of plasma. Different electric discharges provide various mechanisms and conditions of the plasma formation and generate plasma with absolutely different parameters, electron temperatures, and concentrations, which can be used in numerous different applications. The term *gas discharge* initially defined the process of *discharge* of a capacitor into a circuit containing a gas gap between two electrodes. If the voltage between the electrodes is sufficiently large, a breakdown occurs in the gap, the gas becomes a conductor, and the capacitor discharges. This is exactly what occurs in our application.

The main arc-discharge zone located between the electrode layers is called the positive column. The plasma of the arc-discharge positive column can be in quasi equilibrium and in nonequilibrium, depending on the gas pressure. Thus, a nonequilibrium dc plasma can be generated not only in glow discharges, but also in arcs at low pressures, whereas quasi-equilibrium dc plasma can only be generated in electric arcs, which is why electric arcs are usually considered to be a classical example of quasi-equilibrium thermal plasma [31]. The typical ranges of the plasma parameters for the thermal and nonthermal arc discharges are outlined in Table 1.

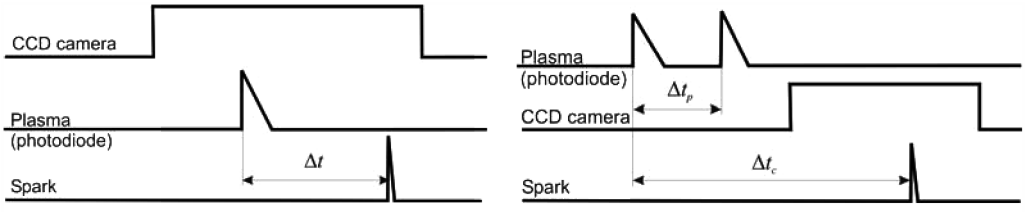

a) Single plasma discharge **b) Two plasma discharges**

Fig. 4 Synchronization sketch of the experiments.

Table 1 Typical ranges of thermal and nonthermal arc-discharge plasma parameters

Discharge plasma parameter	Thermal arc discharge	Nonthermal arc discharge
Gas pressure	0.1–100 atm	10^{-3}–100 torr
Arc current	30 A–30 kA	1–30 A
Cathode current density	10^4–10^7 A/cm^2	10^2–10^4 A/cm^2
Voltage	10–100 V	10–100 V
Power per unit length	>1 kW/cm	<1 kW/cm
Electron density	10^{15}–10^{19} cm^{-3}	10^{14}–10^{15} cm^{-3}
Gas temperature	10,000–20,000 K	300–6000 K
Electron temperature	1–10 eV	1–10 eV

As the table shows and as is clear from their names, thermal arcs operating at high pressures and temperatures are much more energy-intensive. They have higher currents and current densities and higher power per unit length; therefore, these discharges are sometimes referred to as high-intensity arcs. The thermal discharges are usually powerful, easily sustained at high pressures, and operate close to the thermodynamic equilibrium and are not chemically selective. The nonthermal discharges are very selective with respect to plasma chemical reactions and can operate very far from the thermodynamic equilibrium with very high energy efficiency, but usually with limited power. The thermal discharges apply in our application.

High currents in electric-arc discharges can induce relatively high magnetic fields and thus discharge compression effects in the magnetic field. The body forces acting on axisymmetric arcs are illustrated in Fig. 5. Assuming that the current density j in the arc channel is constant, the azimuthal magnetic field B_θ inside an arc can be expressed as

$$B_\theta(r) = \tfrac{1}{2}\mu_0 jr, \qquad r \le r_0 \tag{1}$$

where μ_0 is the magnetic permeability of the medium. This magnetic field results in a radial body force directed inward and tending to pinch the arc. The magnetic body force can be found as a function of the distance r from the discharge axis as

$$\boldsymbol{F} = \boldsymbol{j} \otimes \boldsymbol{B}, \qquad F_r(r) = -\tfrac{1}{2}\mu_0 j^2 r \tag{2}$$

The cylindrical arc channel, in which the expansionary kinetic pressure of plasma p is balanced by the inward radial magnetic body force $\boldsymbol{F}$, is called the Bennet pinch. The equations of this balance can be expressed as

$$\nabla p = \boldsymbol{j} \otimes \boldsymbol{B}, \qquad \frac{\mathrm{d}p}{\mathrm{d}r} = -jB_\theta \tag{3}$$

Together with the formula of the azimuthal magnetic field B_θ, this leads to the relation for pressure distribution inside the Bennet pinch of radius r_0:

$$p(r) = \tfrac{1}{4}\mu_0 j^2\left(r_0^2 - r^2\right) \tag{4}$$

The corresponding maximum pressure (on the axis of the channel) can be rewritten in terms of the total current $I = j\pi r_0^2$ as

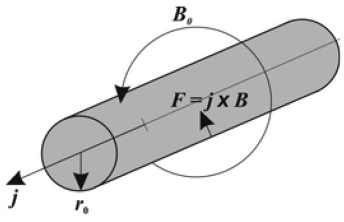

Fig. 5 Radial body forces on the cylindrical arc channel.

$$p_a = \frac{1}{4}\mu_0 j^2 r_0^2 = \frac{\mu_0 I^2}{4\pi r_0^2} \tag{5}$$

Although the Bennet-pinch-effect pressure is usually small with respect to the total pressure, it can initiate electrode jets, which are intensive gas streams that flow away from the electrodes. Additional gas pressure related to the Bennet-pinch effect is inversely proportional to the square of the arc-channel radius. Also, the radius of the arc-channel attachment to the electrode ($r_0 = b$) is less than that corresponding to the positive column ($r_0 = a$). This results in the development of an axial pressure gradient that drives neutral gas along the arc axis away from the electrodes. Assuming that $b \ll a$, the jet dynamic pressure, and thus the jet velocity v_{jet}, can be found from the following simple equation:

$$\Delta p \approx \frac{\mu_0 I^2}{4\pi b^2} = \frac{1}{2}\rho v_{\text{jet}}^2 \tag{6}$$

where ρ represents the plasma density. The electrode-jet velocity can be expressed as the function of the arc current and the radius of the arc attachment to the electrode. Using the air magnetic permeability, a total current of 500 A, and an arc-channel attachment of 0.1 mm, a jet velocity of about 1500 m/s can be reached, which is realistic in our application.

The use of the energy-conservation principle that electric energy is converted into hydrodynamic energy enables us to define the artificial modeling of the plasma discharge for the numerical simulation. The plasma acts as a transverse hot jet over a certain surface S_p during a certain length of time, which vanishes in the following equation:

$$UI = \rho_p S_p v_{\text{jet}}^3 \tag{7}$$

The term $\rho_p S_p v_{\text{jet}}$ represents the mass-flow rate of the modeled plasma discharge, and it is used as boundary condition in the numerical simulations.

V. Numerical Simulations

Numerical simulations of the interaction of the modeled plasma discharge with the projectile crossflow are conducted by means of the CFX-TASCflow code [32]. As demonstrated in the previous section, the artificial modeling of the plasma discharge can be done by a transverse hot jet. This kind of simplification (modeling the plasma-discharge process more or less correctly) is done before starting computations in which the complex magnetohydrodynamic process is taken into account.

The fluid solver is based on the Reynolds-averaged Navier–Stokes equations and provides solutions for the transient, compressible, and turbulent ideal gas flow. The shear-stress transport (SST) two-equation model of turbulence [33] is used to provide a link between the turbulent transport of momentum and energy and the mean flow variables and fluid properties. Furthermore, the SST turbulence model automatically detects and switches from the scalable wall functions to a low-Reynolds-number near-wall formulation as the grid is refined. The software uses block-structured nonorthogonal grids to discretize the domain.

The computation is conducted using a first-order discretization scheme in space and a second-order discretization scheme in time. Only one iteration per time step is applied to the computation, because this study is undertaken to examine the feasibility of the concept; however, the lack of relaxation iterations during one time step could produce oscillations on the computational results. The flowfield disturbed by the transverse hot jet is calculated for a duration of 50 μs by using a time step of 10^{-8} s.

A. Numerical Accuracy

A detailed study on supersonic generic projectiles and missiles was conducted in 2002 to examine the influence of turbulence models and grid refinements on numerical results [34,35]. The

flowfield around different forebodies at several Mach numbers and angles of attack were computed, including flow separation in some cases. The analysis of the huge amount of computational results concludes that the accuracy of the prediction of the surface pressure, axial force, normal force, and pitching-moment coefficients is estimated to be $\pm 2\%$. Moreover, the computed global coefficients were compared with the experimental coefficients: the axial-force coefficient and the derivative of the normal-force coefficient are overestimated by 2 and 8%, respectively; the derivative of the pitching moment is underestimated by 5%.

The physics of the interaction between a transverse jet with the crossflow of a missile is widely described in [7–11] and in [36]. The numerical accuracy is particularly highlighted in [10,36]; the computation using a fine grid and the SST turbulence model predicts the boundary-layer separation, the jet expansion, and the recompression shock with an accuracy that is of the same order of magnitude as that encountered in the experiments.

B. Projectile Geometry

The numerical study is made for a projectile of a 20-mm caliber D without any angle of attack. Figure 6 shows the sketch of the projectile geometry, which consists of a cone nose, a cylindrical midsection, and a cone trunk. The location of the electrodes is identical to that defined by the experiments. The studied configuration has a symmetry plane, and thus the numerical study is performed for half the computational domain. The computation is only focused on the flow around the body, so that the projectile wake is not meshed.

C. Grid Specifications

Several numerical simulations were performed in 2002 on an isolated cone to check different meshes. Only the result obtained by using the finest mesh is presented in this paper. The use of a finer computational mesh is now possible as a result of increased computational resources, but the accuracy gained is not justified in view of the hypotheses used in the plasma modeling.

The computational domain is limited by the surfaces for which the boundary conditions are fixed. The projectile is located within a half-cylindrical volume. The conical upstream surface of about 30 deg is located only at a half-projectile diameter ahead of the missile nose, because the external flow is supersonic. The conical downstream surface is located at the end of the projectile surface. The cylindrical surface is built at a distance of two calibers from the projectile symmetry axis.

The mesh of the half-plane of symmetry is composed of a block with 175 and 45 nodes in the longitudinal and radial directions, respectively. That block has 25 nodes distributed along the projectile circumference; the nodes are located closer to one another on the side of the transverse hot jet. In addition, a grid refinement is realized near the jet exit: a block of $151 \times 43 \times 19$ nodes distributed, respectively, in the longitudinal, radial, and circumferential directions is embedded in the previous block. The boundary layer is resolved with a minimum of 15 nodes in the direction normal to the wall. The distance between a node located on the projectile surface and the first node located in the flow is 75 μm. That distance is reduced to 25 μm in the refinement region. Therefore, the mesh is built in such a way that the y^+ values range from 5 to 60 (mean value of 13), allowing the use of the near-wall treatment.

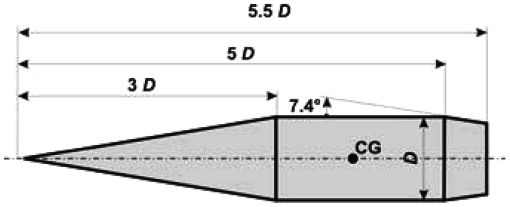

Fig. 6 Projectile geometry for the numerical simulation.

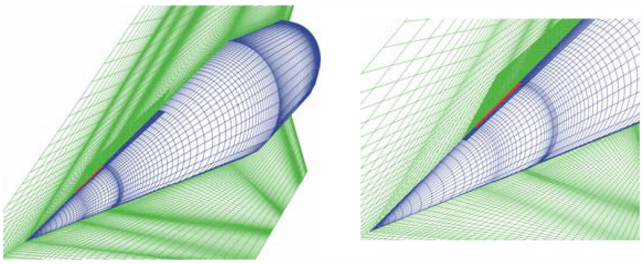

Fig. 7 Mesh of the symmetry plane and of the projectile surface.

Figure 7 shows (on the left) the mesh of the symmetry plane and of the projectile surface. The zoom near the nosetip (on the right) depicts the region in which the transverse hot-jet conditions are fixed. The node density is large in the regions of large gradients (in particular, within the region in which the jet plume develops).

D. Boundary Conditions

The thermal arc discharge is modeled by the use of a high temperature and a mass-flow rate. All computations cannot be presented and discussed within this paper, but in brief, the temperature rise produces the reduction of the wall shear stress; when added to the mass-flow rate, they produce the shock-wave distortion. With no accurate information about the energy consumption dissipated during the plasma discharge (it is difficult to measure the current), the computation seems to be an indirect way to access to that quantity via the energy-conservation principle equation (7). The computation is made for a perfect gas; the transverse hot jet is defined by considering a small region Sp of the projectile surface that produces the temperature rise and the mass-flow rate $\rho_p S_p v_{\text{jet}}$ increase during a certain length of time.

The projectile surface is assumed to be a smooth wall. A symmetry boundary condition is applied to the symmetry plane of the problem. The boundary conditions of the crossflow are nearly the same as the conditions encountered in the shock tube. The fluid enters the computational domain through the upstream conical surface at a given Mach number. The Mach number ($M_\infty = 4.65$), the static temperature ($T_\infty = 238.5$ K), and the static pressure ($P_\infty = 0.4106 \times 10^5$ Pa) are set at the nodes of inlet regions. With no information about the turbulent aspect of the crossflow, one specifies that the turbulent kinetic energy k and its dissipation rate ϵ are constant along inlet regions; this is done by fixing the turbulence rate ($Tu = 1\%$) and the eddy length ($Lt = 2$ mm). A supersonic outlet is used for the nodes of outlet regions. The boundary conditions on the cylindrical surface limiting the computational domain are of the opening type, which means that the solver implicitly determines the incoming and the outgoing regions of the flow.

VI. Results

A. Experimental Results

The experimental conditions are those simulating a projectile flying at an altitude of about 5 km at a Mach number of 4.57 (± 0.02), except for the first series of tests, in which the air remains at rest.

1. *One Plasma Discharge in Air at Rest*

Several tests of a plasma discharge are made in air at rest at an ambient pressure ranging from 1.5×10^3 Pa to 10^5 Pa. They are carried out to analyze the plasma-discharge generation at pressures representing the medium at different projectile altitudes. Figure 8 shows three interferogram pictures taken 4 μs after the plasma discharge (delay Δt). Two phenomena are recorded on each picture: the plasma discharge characterized by the white light and the medium disturbance characterized by the variation of the gray color. The shock wave is clearly highlighted at 5×10^4 Pa, whereas it does not exist at 3×10^3 Pa. These tests prove that the voltage necessary to disrupt the electric barrier between the electrodes is higher in a high-pressure medium than in a very-low-pressure medium, as

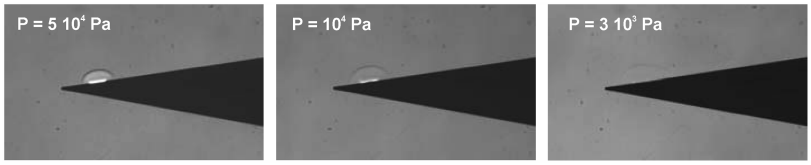

Fig. 8 Interferogram of a plasma discharge in air at rest.

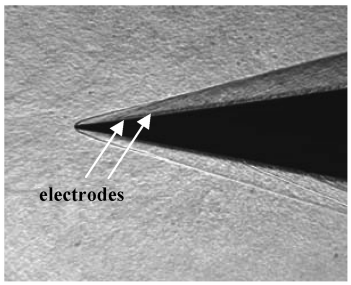

Fig. 9 Interferogram of the steady-state flowfield with no plasma discharge.

expected. In a high-pressure medium, the plasma-discharge behavior looks like that of a pulsed hot jet.

2. No Plasma Discharge in a Supersonic Crossflow

A test is carried out without any plasma discharge to take an interferogram picture as a reference (Fig. 9). The flowfield around the conical part of the model is only visualized. The shock wave attached to the nosetip is perfectly visible. The conical part of the model is built using different materials and, inevitably, the electrodes are not perfectly flush with the conical surface. This fact and other surface bumps produce disturbances in the flowfield that are visible on the picture.

3. One Plasma Discharge in a Supersonic Crossflow

The upstream conditions are almost the same in all tests: the flow velocity is 1444 m/s (± 7 m/s), the static temperature is 239 K (± 2 K), and the static pressure is 0.409×10^5 Pa ($\pm 7 \times 10^2$ Pa). The experimental conditions are those simulating a projectile flying without any angle of attack. A series of experiments is carried out to vary the delay Δt.

Figure 10 presents eight interferograms to analyze the evolution of the disturbance generated by the plasma discharge. The analysis of the pictures taken at $\Delta t = 2$ and 4 μs shows an inversion of the vertical gradient direction of the interferometer: flow disturbances characterized by bright shades on the $\Delta t = 2$ μs picture appear as dark shades on the $\Delta t = 4$ μs picture, and vice versa. The white light of the plasma discharge is visible on every , because the CCD camera shutter is opened before the plasma-discharge production. This analysis is necessary to distinguish the plasma-discharge production from the disturbance generated by it.

The formation and the growth of the disturbance and its propagation between the model conical surface and the attached

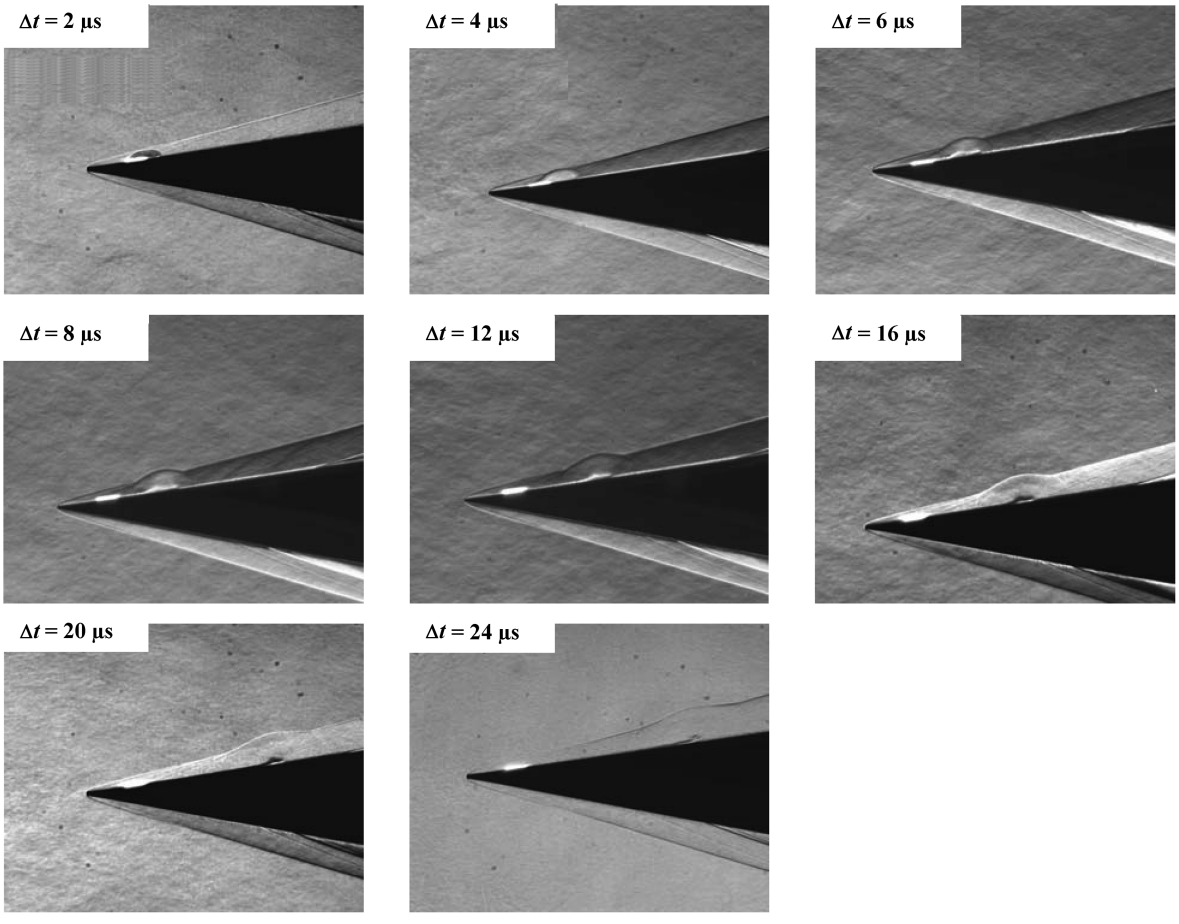

Fig. 10 Evolution of the disturbance generated by one plasma discharge.

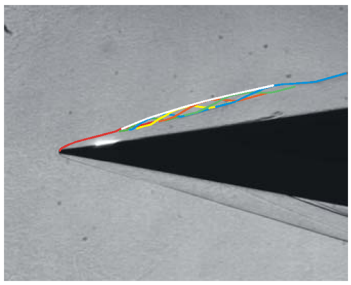

Fig. 11 Envelope of contours of the distorted shock wave.

shock wave are clearly highlighted. The shock-wave geometry and the boundary layer are locally modified by the disturbance. After 24 μs, the mean convection velocity of the disturbance is nearly 1250 m/s, which is about 10% lower than the flow velocity determined behind the shock wave by the tables given in [37]. The maximum voltage amplitude of the discharge is nearly 18 kV and its duration is about 1.5 μs.

Figure 11 depicts the superposition of the successive contours (plotted using the pictures taken from $\Delta t = 4$ to 24 μs) of the distorted shock wave on the picture in Fig. 10 for $\Delta t = 24$ μs. The envelope of these seven contours is represented by the white curve, and it could correspond to the projectile shock wave if successive plasma discharges were produced at a sufficiently high rate. The same kind of effect could be obtained by increasing the duration of the single plasma discharge, but the energy required should be higher.

The first series of experiments clearly shows the possibility of distorting the shock wave attached to a supersonic projectile by using a high-voltage discharge. The flow structure between that shock wave and the conical surface of the projectile model is therefore modified. A higher energy delivered at the electrode bounds will easily increase the disturbance intensity. However, it is necessary to maintain the flow disturbance by plasma discharge during a certain length of time (a few milliseconds) to obtain a larger distortion of the shock wave. As mentioned earlier, this type of system should allow the production of several series of plasma discharges at required instants, provided that enough energy is stored in the projectile. Thus, the repetition of the flow disturbances leads to an asymmetry of the pressure distribution along the projectile and, consequently, gives an angle of attack to the projectile. The challenge of this concept consists of a repeatable and controlled plasma discharge to obtain the required angle of attack.

When the projectile has an angle of attack due to the action of plasma discharges, it could be stabilized along the new trajectory by using the same kind of system. Some experiments are carried out under the same conditions as before, except that the angles of attack are of -5 and $+5$ deg.

Figure 12 presents the flow structure around the projectile model at angles of attack of -5 and $+5$ deg. The pictures are taken so that $\Delta t = 12$ μs, and they prove that it is possible to disturb the flow on the side of the plasma discharge even if the projectile has an angle of attack. This is interesting for the projectile steering, because the angle of attack can be amplified, yet the projectile can be stabilized.

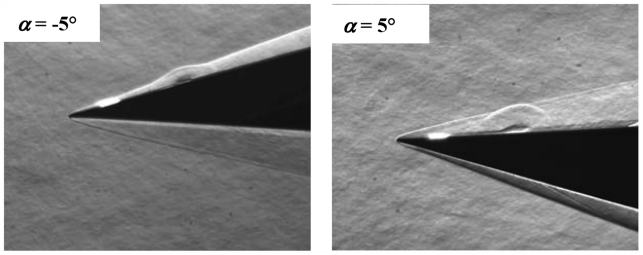

Fig. 12 Disturbance generated by one plasma discharge at $\Delta t = 12$ μs.

4. *Two Plasma Discharges in a Supersonic Crossflow*

The upstream conditions are almost the same in all tests: the flow velocity is 1493 m/s ($\pm$14 m/s), the static temperature is 258 K ($\pm$9 K), and the static pressure is 0.466×10^5 Pa ($\pm 3 \times 10^3$ Pa). A series of experiments is carried out by changing the delay Δt_p between the two plasma discharges. Another series is conducted by varying the delay Δt_c between the first plasma discharge and the selected spark. The picture in Fig. 9 is useful as a reference for the analysis of the results.

The interferogram pictures of Fig. 13 are taken by activating the spark 13 μs after the first plasma discharge ($\Delta t_c = 13$ μs) for three delays Δt_p. The synchronization is achieved in accordance with that described in Sec. III.E.2. The absence of the plasma light proves that the extinguishing occurs before the spark was generated. The analysis shows that the discharges are well separated optically when $\Delta t_p = 3$ μs.

For $\Delta t_p = 1.6$ and 2.7 μs, several tests show that the disturbances produced by the plasma discharges are not optically distinct. The reason is that the theoretical distance between the two disturbances is less than 0.5 mm for $\Delta t_p = 1.6$ μs, which corresponds to 0.3 mm in the picture, based on the length scaling.

Figure 14 shows the voltage discharge of the capacitors measured during two experiments corresponding to $\Delta t_p = 1.7$ and 7.1 μs. A current measurement could help to better analyze the phenomenon. The discharges are well separated electrically, even though it is optically not the case for $\Delta t_p = 1.6$ μs. The maximum voltage amplitude of the first discharge is nearly 15 kV and its duration is about 1.5 μs. The amplitude of the second discharge is twice as low as that of the first discharge, even though the generators are identical; the differences are due to the addition of the diode resistance to the circuit of the second generator and to the change of the flow variables near the electrodes, which has an influence on the strain conditions.

Figure 15 presents the evolution of the disturbances generated by two plasma discharges separated by $\Delta t_c = 6.0$ μs. The second discharge generates a lower disturbance than the first discharge, as expected by analyzing the graph of Fig. 14. The disturbances seem to move at the same velocity.

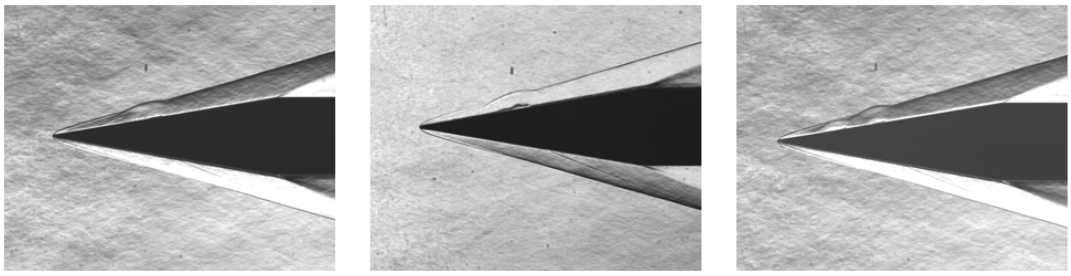

Fig. 13 Disturbances generated by two plasma discharges at $\Delta t_c = 13$ μs.

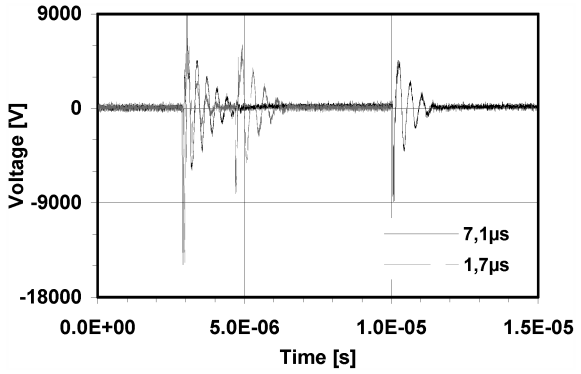

Fig. 14 Voltage measurement in the presence of two plasma discharges at $\Delta t_p = 1.7$ μs and 7.1 μs.

B. Computational Results

The steady-state computation of the projectile flying without any angle of attack and without any transverse jet is the first step of the study. This state corresponds to the instant $t = 0$, at which the jet production starts to be applied. The second step of the study is to run the transient computation from $t = 0$, with the continuous application of the transverse jet during 50 μs. Figure 16 presents the density field in the symmetry plane and on the projectile surface for three instants. The density scale ranges from 0.02 to 1.25 kg/m^3.

The shock wave attached to the nosetip, the expansion wave due to the junction of the conical nose with the cylindrical part of the forebody, and the boundary-layer thickness are perfectly highlighted in Fig. 16. The evolution of the disturbance in the flowfield and on the projectile surface is also well highlighted. The geometry of the attached shock wave starts to be distorted on the side of the plasma discharges as soon as the jet generation begins. The density near the jet widely decreases at the beginning of the process. The density change extends inside the flowfield and on the upper side of the projectile surface as time goes along. At $t = 50$ μs, the boundary layer on the upper side of the cylindrical part thickens. The density field does not change on the lower side of the projectile surface. These changes in the density field around the projectile cause the asymmetry of the flowfield between the upper and the lower sides, leading to an asymmetry of the pressure distribution on the projectile. Consequently, a normal force is created in the direction of the symmetry plane, and its action generates a pitching moment.

C. Experimental and Computational Results Comparison

The numerical simulation allows the distorted shock-wave trace to be obtained in the symmetry plane. Figure 17 presents that computed trace superimposed on the experimental trace from Fig. 11. It must be kept in mind that the computed trace is obtained after 50 μs and that the experimental trace is deduced after a 24-μs analysis of the series of tests. The graph of the numerical simulation shows two isovelocity contours: one represents the trace of the distorted shock wave and the other represents the limit of the boundary layer. The graph of the experiments shows the envelope of the contours, and it could correspond to the projectile shock wave if successive plasma discharges were produced at a sufficiently high rate.

The numerical simulation allows the determination of the thrust force Fp produced by the transverse hot jet and its pitching moment $My/0_{(Fp)}$, as well as the induced normal force Fn and its pitching moment $My/0_{(Fn)}$. Figure 18 presents the evolution of the total force and pitching moment,

$$F = Fp + Fn, \qquad My/0 = My/0_{(Fp)} + My/0_{(Fn)}$$

calculated at nosetip 0. The total force and the total pitching moment are of opposite signs. Some oscillations appear after 30 μs, which could be due to the lack of relaxation iterations; a tendency curve is plotted for each quantity. Table 2 presents the results of the numerical simulation obtained without any jet and with the action of the transverse hot jet after 50 μs. The drag force Fx is reduced by the action of the modeled plasma, a result that is already known [16].

As represented in the sketch of Fig. 19, the total force and the pitching moment combine favorably and tend to give an angle of attack to the projectile, which leads to the desired goal. This steering system can be interesting even when the loads are low, because a slight controlled asymmetry of the flowfield due to an action near the nosetip can destabilize the projectile when it flies near its stability limit. A second action of plasma discharge would stabilize the projectile again on the corrected trajectory.

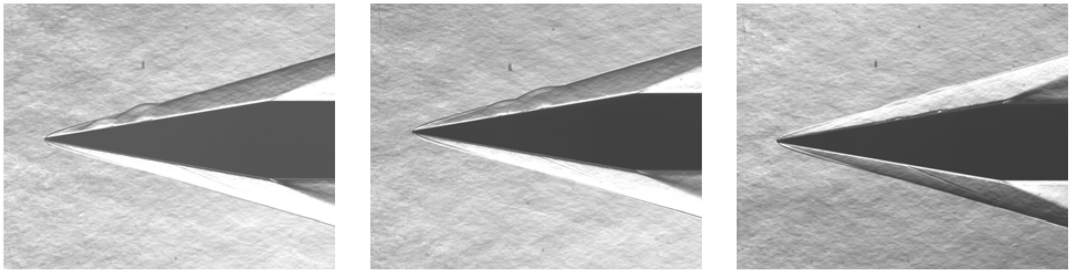

Δt_c = 13 µs **Δt_c = 19 µs** **Δt_c = 25 µs**

Fig. 15 Disturbances generated by two plasma discharges separated by $\Delta t_p = 6.0$ μs.

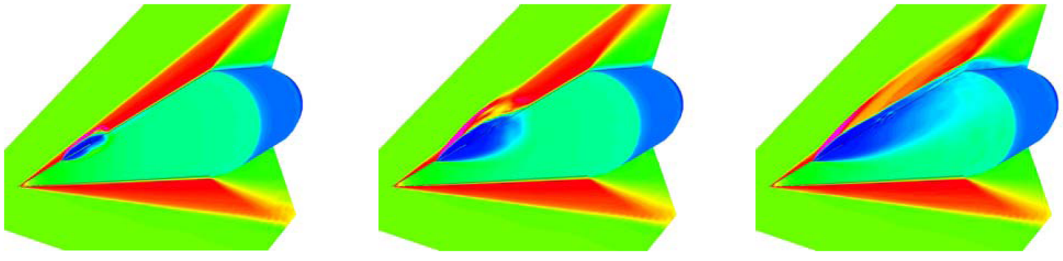

t = 2.5 µs **t = 10 µs** **t = 50 µs**

Fig. 16 Density field in the symmetry plane and on the projectile surface with hot-jet modeling.

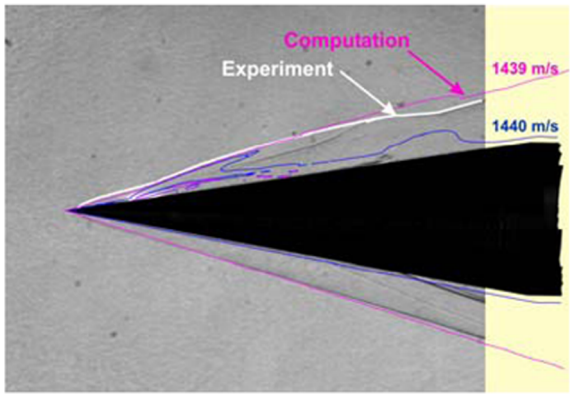

Fig. 17 Experimental and computed traces of the distorted shock wave.

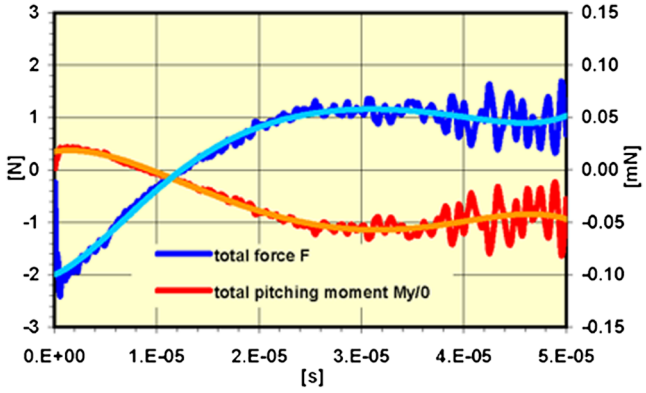

Fig. 18 Evolution of the force and the moment exerted on the projectile.

VII. Conclusions

The shock tube used as a wind tunnel is a facility that is well adapted to the experimental study of the steering of a supersonic projectile flying in the conditions encountered between the ground level and 10 km of altitude. The visualization of the interaction between a plasma discharge and the crossflow of a projectile and the measurement of the voltage evolution in the plasma discharge were the main goal of the experiments presented in this paper. The visualizations prove that plasma discharges can be produced at the tip of a projectile flying at a Mach number of 4.5 in conditions encountered at a low altitude, which is not trivial at all.

A plasma discharge produces a disturbance between the projectile surface and the shock wave attached to its conical nose. The perturbation is strong enough to distort the attached shock wave. When established, the perturbation is transported along the projectile surface, causing the local modification of the aerothermodynamic variables. Experiments were also carried out with two plasma discharges generated independently between the same electrode couple.

The analysis of the dynamic effects in electric arcs justifies the modeling of the plasma discharge by a transverse hot jet for the numerical simulation. The qualitative comparison between the numerical results and the interferogram pictures shows that the computation is able to reproduce the structure of the flowfield disturbed by plasma discharges. The numerical simulation allows the determination of the induced aerodynamic loads on the projectile, and the results demonstrate the favorable combination of the force

Table 2 Aerodynamic forces and moment

Fp, N	$My/0_{(Fp)}$, mN	Fx, N	Fn, N	$My/0_{(Fn)}$, mN	Xcp, m
——	——	21.1	——	——	——
−0.39	0.0018	20.3	1.46	−0.0546	0.049

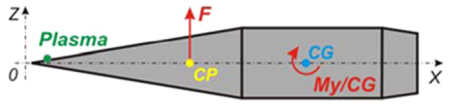

Fig. 19 Force and moment exerted on the projectile.

and of the pitching moment that tend to give an angle of attack to the projectile.

This study, proving the feasibility of the proposed concept, completes the patent issued in France in January 2005 and in the United States in February 2006. Since the present study, some other investigations have been under study, such as on the influence of the energy, the duration of the plasma discharge, the repeatability of the discharges, the interelectrode distance, and the integration of the generator into a projectile. This concept of plasma actuator can be applied to all supersonic or hypersonic flying vehicles, such as projectiles, missiles, unmanned aerial vehicles, micro air vehicles, waveriders, etc.

Acknowledgments

The authors thank the Aerothermodynamics and Shock Tube Department staff for its efficiency. They especially thank F. Seiler, head of the department, for the benevolence that he granted in the realization of the experiments.

References

[1] Dupuis, A., Berner, C., and Fleck, V., "Aerodynamic Characteristics of a Long-Range Spinning Artillery Shell, Part 1: From Aeroballistic Range Free-Flight Tests," 21st International Symposium on Ballistics, Adelaide, Australia, French–German Research Inst. of Saint-Louis Paper PU-629/2004, Apr. 2004.

[2] Dupuis, A., and Berner, C., "Aerodynamic Aspects of a Grid Finned Projectile at Subsonic and Supersonic Velocities," 19th International Symposium on Ballistics, French–German Research Inst. of Saint-Louis Paper PU-623/2002,May 2001.

[3] Berner, C., and Dupuis, A., "Wind Tunnel Tests of a Long-Range Artillery Shell Concept," AIAA Atmospheric Flight Mechanics Conference and Exhibit, Monterey, CA, AIAA Paper 2002-4416, Aug. 2002.

[4] Berner, C., Fleck, V., and Dupuis, A., "Experimental and Computational Analysis for a Long-Range Spinning Artillery Shell with Lifting Surfaces," 20th International Symposium on Ballistics, Orlando, FL, French–German Research Inst. of Saint-Louis Paper PU-634/2002, Sept. 2002.

[5] Berner, C., and Dupuis, A., "Wind Tunnel Tests of a Grid Finned Projectile Configuration," 39th AIAA Aerospace Sciences Meeting and Exhibit, Reno, NV, AIAA Paper 2001-105, Jan. 2001.

[6] Srulijes, J., Seiler, F., Hennig, P., and Gleich, P., "Visualisierung der Umströmung von Lenkflügeln im Stoßrohr-Windkanal Bei Realen Atmosphärischen Strömungsbedingungen," French–German Research Inst. of Saint-Louis Rept. RV 229/2004, Saint-Louis, France, 2004.

[7] Gnemmi, P., and Seiler, F., "Interaction of a Lateral Jet with the Projectile External Flow," 2000 AIAA Atmospheric Flight Mechanics Conference and Exhibit, Denver, CO, AIAA Paper 2000-4196, Aug. 2000.

[8] Schäfer, H. J., Augenstein, E., Esch, H., and Emunds, H., "Experimental Investigation of Transverse Jet Interaction on a Missile Body Using Laser Velocimetry and Flow Visualization," 19th International Congress on Instrumentation in Aerospace Simulation Facilities, Cleveland, OH, French–German Research Inst. of Saint-Louis Paper PU-635/2001, Aug. 2001.

[9] Seiler, F., Gnemmi, P., Ende, H., Schwenzer, M., and Meuer, R., "Jet Interaction at Supersonic Crossflow Conditions," *Shock Waves*, Vol. 13, No. 1, July 2003, pp. 13–23. doi:10.1007/s00193-003-0189-y

[10] Gnemmi, P., and Schäfer, H. J., "Experimental and Numerical Investigations of a Transverse Jet Interaction on a Missile Body," 43rd AIAA Aerospace Sciences Meeting and Exhibit, Reno, NV, AIAA Paper 2005-52, Jan. 2005.

[11] Havermann, M., Seiler, F., Ende, H., and George, A., "Untersuchungen im Stossrohr-Windkanal zur Steuerung Eines Hochgeschwindigkeits-Flugkörpers mit Seitenstrahlen," French–German Research Inst. of Saint-Louis Rept. RV 232/2004, Saint-Louis, France, 2004.

[12] Wey, P., Berner, C., and Sommer, E., "Guidage et Pilotage de Munition d'Artillerie Sol-Air: Une Introduction au Projet GSP," French–German Research Inst. of Saint-Louis Rept. RV 240/2005, Saint-Louis, France, 2005.

[13] Gnemmi, P., Samirant, M., and Charon, R., French–German Research Inst. of Saint-Louis, Saint-Louis, France, French Patent for "Pilotage d'un Projectile par Décharge Plasma," No. 02 12906, filed 17 Oct. 2002, issued 7 Jan. 2005.

[14] Gnemmi, P., Samirant, M., and Charon, R., French–German Research Inst. of Saint-Louis, Saint-Louis, France, U.S. Patent for "Projectile Steering by Plasma Discharge," No. 7,002,126 B2, filed 17 Oct. 2003, issued 21 Feb. 2006.

[15] Menart, J., Shang, J. S., Atzbach, C., Magoteaux, S., Slagel, M., and Bilheimer, B., "Total Drag and Lift Measurements in a Mach 5 Flow Affected by a Plasma Discharge and a Magnetic Field," 43rd AIAA Aerospace Sciences Meeting and Exhibit, Reno, NV, AIAA Paper 2005-947, Jan. 2005.

[16] Leonov, S. B., Savelkin, K. V., Yarantsev, D. A., and Yuriev, A. S., "Experimental Study of Electro-Discharge Plasma Impact on Drag and High-Speed Flow Structure," *Eighth International Symposium on Fluid Control, Measurement and Visualization* [CD-ROM], China Aerodynamics Research Society and China Society of Theoretical and Applied Mechanics, Beijing, 22–25 Aug. 2005.

[17] Shang, J. S., Surzhikov, S. T., Kimmel, R., Gaitonde, D., Menart, J., and Hayes, J., "Plasma Actuators for Hypersonic Flow Control," 43rd AIAA Aerospace Sciences Meeting and Exhibit, Reno, NV, AIAA, 10–13 Jan. 2005.

[18] Kuo, S. P., and Bivolaru, D., "Electric Discharge in the Presence of Supersonic Shocks," *Physics Letters A*, Vol. 313, Nos. 1–2, June 2003, pp. 101–105.
doi:10.1016/S0375-9601(03)00721-7

[19] Kuo, S. P., "Conditions and a Physical Mechanism for Plasma Mitigation of Shock Wave in a Supersonic Flow," *Physica Scripta*, Vol. 70, Nos. 2–3, 2004, pp. 161–165.
doi:10.1088/0031-8949/70/2-3/014

[20] Fomin, V. M., Tretyakov, P. K., and Taran, J. P., "Flow Control Using Various Plasma and Aerodynamic Approaches," *Aerospace Science and Technology*, Vol. 8, No. 5, 2004, pp. 411–421.
doi:10.1016/j.ast.2004.01.005

[21] Leonov, S. B., Bityurin, V. A., Yarantsev, D. A., Napartovich, A. P., and Kochetov, I. V., "Plasma-Assisted Ignition and Mixing in High-Speed Flow," 8th International Symposium on Fluid Control, Measurement and Visualization, Chengdu, China, 22–25 Aug. 2005.

[22] Jacob, J., Rivir, R., Carter, C., and Estevadeordal, J., "Boundary Layer Flow Control Using AC Discharge Plasma Actuators," 2nd AIAA Flow Control Conference, Portland, OR, AIAA Paper 2004-2128, 2004.

[23] Hong, D., Magnier, P., Bauchire, J. M., Leroy-Chesneau, A., and Pouvesle, J. M., "Preliminary Study of Electric Discharges for Airflow Controls," 8th International Symposium on Fluid Control, Measurement and Visualization, Chengdu, China, 22–25 Aug. 2005.

[24] Corke, T. C., and Post, M. L., "Overview of Plasma Flow Control: Concepts, Optimization, and Application," 43rd AIAA Aerospace Sciences Meeting and Exhibit, Reno, NV, AIAA Paper 2005-563, Jan. 2005.

[25] Coduti, G., "Etude de l'Interaction d'Une Onde Électromagnétique avec un Plasma d'Air à Température Ambiante," Ph.D. Dissertation, Univ. of Paris XI, Paris, Jan. 2005.

[26] Patz, G., "Das Hyperschallstossrohrlabor des ISL, 3. Teil: Stossrohr B", French–German Research Inst. of Saint-Louis Rept. N 30/70, Saint-Louis, France, Sept. 1970.

[27] Patz, G., "Das Hyperschallstossrohrlabor des ISL, 2. Teil: Stossrohr A", French–German Research Inst. of Saint-Louis Rept. N 27/71, Saint-Louis, France, Nov. 1971.

[28] Oertel, H., "*Stossrohre*," Springer–Verlag, New York, 1966.

[29] Stenzel, A., "Generator für 20-kV-Impuls", French–German Research Inst. of Saint-Louis Rept. NI 74/3, Saint-Louis, France, 1974.

[30] Smeets, G., "Interferometry," French–German Research Inst. of Saint-Louis Rept. CO 214/90, Saint-Louis, France, May 1990.

[31] Fridman, A., and Kennedy, L. A., *Plasma Physics and Engineering*, Taylor and Francis, New York, 2004.

[32] CFX-TASCflow, Software Package, Ver. 2.12, ANSYS Canada Ltd., Waterloo, Ontario, Canada, 2003.

[33] Menter, F. R., "Two-Equation Eddy-Viscosity Turbulence Models for Engineering Application," *AIAA Journal*, Vol. 32, No. 8, 1994, pp. 1598–1605.

[34] Gnemmi, P., "Influence des Modèles de Turbulence sur la Prévision de l'Aérothermodynamique d'un Projectile de 155 mm," French–German Research Inst. of Saint-Louis Rept. CR/RV 458/2002, Saint-Louis, France, 2002.

[35] Gnemmi, P., "Influence des Modèles de Turbulence sur la Prévision de l'Aérothermodynamique de l'Avant-Corps d'Engins Génériques d'un Missile," French–German Research Inst. of Saint-Louis Rept. CR/RV 475/2002, Saint-Louis, France, 2002.

[36] Gnemmi, P., Eichhorn, A., Leopold, F., Schäfer, H. J., Emunds, H., Esch, H., and Gülhan, A., "Experimental and Computational Study of the Interaction Between a Lateral Jet and the Supersonic External Flow on a Generic Missile Body," NATO-RTO Symposium on Innovative Missile Systems, RTO-MP-AVT-135, NATO Research and Technology Organization, Paper 31, May 2006.

[37] Jones, D. J., "Tables of Inviscid Supersonic Flow About Circular Cones at Incidence, $\gamma = 1.4$," AGARD, Rept. AGARD-96-137/1, Neuilly-sur-Seine, France, Nov. 1969.

K. Powell
Associate Editor